Theoretical Study of the Complex-Forming CH + H_2 → CH_2 + H Reaction†

Jordi Mayneris,‡,§ Amaia Saracibar,||,⊥ Evelyn M. Goldfield,|| Miguel González,§ Ernesto García,⊥ and Stephen K. Gray*,‡

Chemistry Division, Argonne National Laboratory, Argonne, Illinois 60439, Departament de Química Física i Centre de Recerca en Química Teòrica, Universitat de Barcelona i Parc Científic de Barcelona, C/Martí i Franquès, 1, 08028 Barcelona, Spain, Department of Chemistry, Wayne State University, Detroit, Michigan 48202, and Departamento de Química Física, Universidad del País Vasco 01006, Vitoria, Spain

Received: November 29, 2005; In Final Form: January 25, 2006

The complex-forming CH + H_2 → CH_2 + H reaction is studied employing a recently developed global potential energy function. The reaction probability in the total angular momentum $J = 0$ limit is estimated with a four-atom quantum wave packet method and compared with classical trajectory and statistical theory results. The formation of complexes from different reactant internal states is also determined with wave packet calculations. While there is no barrier to reaction along the minimum energy path, we find that there are angular constraints to complex formation. Trajectory-based estimates of the low-pressure rate constants are made and compared with experimental results. We find that zero-point energy violation in the trajectories is a particularly severe problem for this reaction.

1. Introduction

The $H_2 + CH(^2\Pi) \rightarrow H + CH_2(\tilde{X}^3B_1)$ reaction and its reverse reaction have been the subject of a number of experimental and theoretical studies, for example, refs 1−8. Being one of the simplest systems involving the methylidyne (CH) radical, it is relevant to gas-phase hydrocarbon combustion. The reaction involves intermediate formation of the methyl radical, $CH_3(\tilde{X}^2A_2'')$. The nature of the complex formation should be interesting because "non-least-motion" paths with CH and H_2 oriented parallel to one another at moderate separations, followed by C_{2v} insertion at shorter separations, are expected to be important.[7,8]

Recently, a global potential energy function, based on high-quality ab initio data, was developed for the CH_3 system and shown to lead to accurate vibrational energy levels.[9] In this paper, we employ this potential energy function to carry out a variety of theoretical calculations on the CH + H_2 reaction. A four-atom wave packet approach[10] is used to estimate the total angular momentum $J = 0$ reaction probability, which is compared to corresponding classical trajectory and statistical theory estimates. The probability of complex formation is also determined for several different reactant internal states and for different total angular momenta, showing that there are indeed angular constraints to complex formation. Finally, rate constants are estimated at the classical trajectory level and compared to experiment.

Note that our work is relevant to the zero-pressure limit of the CH + H_2 reaction. The effect of pressure on the stabilization and the decomposition of CH_3 complexes is an interesting issue that we do not probe here. See, for example, the work of Hippler and co-workers[5,6] who have carried out experimental and theoretical studies focusing on the collisional effects in CH_3 decomposition.

Section II below discusses relevant computational details, section III presents our results, and section IV concludes.

2. Computational Methods

2.1. Potential Energy Function. Details of the global potential energy function employed here are given in ref 9. Briefly, it is an accurate fit to over 75 000 multireference configuration interaction electronic structure points sampling the $CH_3(\tilde{X}^2A_2'')$, $CH_2(\tilde{X}^3B_1)$ + H, and $CH(^2\Pi)$ + H_2 regions and the regions connecting them. The depth of the CH_3 well is 4.8 eV relative to the energy of isolated CH and H_2 at their equilibrium bond distances. On this surface, the CH + H_2 → CH_2 + H reaction is barrierless along the minimum energy path (MEP), with a bare endothermicity of 0.18 eV and a zero-point corrected endothermicity of 0.20 eV. This latter theoretical endothermicity is within 0.055 eV (1.3 kcal/mol) of the experimentally based endothermicity, 0.145 ± 0.006 eV, inferred from Active Thermochemical Tables.[11,12]

Reaction to form CH_2 + H takes place primarily through the formation of intermediate CH_3 complexes. Figure 1 displays the MEP for complex formation. It was obtained by varying the separation between the CH and H_2 center-of-masses, R, and minimizing the potential with respect to the remaining internal coordinates. For $R > 2.51\ a_0$, the MEP corresponds to planar geometries with the CH and H_2 bonds oriented more parallel to one another, in accordance with the early work of Brooks and Schaefer.[7] For $R < 2.51\ a_0$, the MEP corresponds to planar geometries with a C_{2v} type insertion of the CH bond into the H_2 bond. At $R = 2.5\ a_0$, minima corresponding to both the parallel and C_{2v} approaches coexist with the same energy. Each minimum has energy of approximately −0.73 eV, and they are connected via a saddle point at energy ∼0.57 eV. Thus, while

† Part of the special issue "John C. Light Festschrift".

* To whom correspondence should be addressed. E-mail: gray@anchim.chm.anl.gov.

‡ Argonne National Laboratory.

§ Universitat de Barcelona i Parc Científic de Barcelona.

|| Wayne State University.

⊥ Universidad del País Vasco.

10.1021/jp056936h CCC: $33.50
Published on Web 03/11/2006

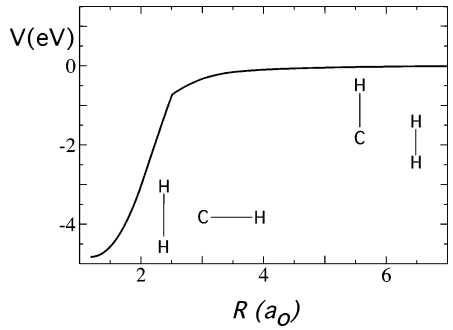

Figure 1. Energy along the MEP (solid curve) corresponding to the formation of CH_3 from CH and H_2 fragments as a function of the separation between fragments, *R*. Schematic diagrams of parallel and C_{2v} approaches are also indicated.

there is no barrier to complex formation in this system, the angular variation along the MEP suggests that not all approaching CH and H_2 fragments will lead to complexes.

2.2. Quantum Dynamics. We employ the real wave packet[13] method along with a diatom + diatom Jacobi coordinates four-atom representation.[10] We restrict these quantum calculations to the total angular momentum $J = 0$ limit with reactants in their zero-point energy (ZPE) states. The wave packet is a function of six nuclear degrees of freedom: the separation of the CH and H_2 centers-of-mass, *R*; the CH and HH internuclear distances, r_{CH} and r_{HH}; and three angular coordinates θ_{CH}, θ_{HH}, and φ. The angular coordinates correspond to the angles made by the CH and HH bonds with the *R* axis and an associated torsional angle. Evenly spaced grids are used to represent r_{HH} and *R*, and parity-adapted angular basis functions or equivalent primitive grids are used to represent the angular degrees of freedom.[10]

As in the treatment of the OH in the previous work on OH + H_2,[10] we assume that the CH bond associated with the reactant CH does not break and describe it with a potential-optimized discrete variable representation (PODVR).[14] This assumption leads to no significant errors in the capture probabilities we calculate, since the subsequent CH_3 complex dynamics is not relevant to them. However, the quantum reaction probabilities we calculate based on this assumption are most likely overestimates of the true ones. The Appendix discusses this in greater detail and develops a simple correction procedure for the reaction probabilities. We assume that the CH bond does not break for reasons of computational efficiency; the reactive quantum dynamics calculations already can require many hours of computational time on a sixteen processor shared-memory parallel node. In the future, we plan to carry out a more extensive calculation with grids for all radial degrees of freedom, employing a wave packet code optimized to run in a massively parallel environment.[15]

Each step of the real wave packet propagation involves evaluating the action of the Hamiltonian operator on the wave packet. Primitive rotational basis functions are used to represent the wave packet when evaluating the action of the rotational kinetic energy, and transformations to and from an angular grid point representation are used to evaluate the action of the potential on the wave packet.[10] The total reaction probability is evaluated on a grid of energies according to a flux analysis[16] based at $r_{HH} = 7\ a_0$. Other numerical aspects, including spatial grids and rotational bases, are listed in Table 1. Many tests with larger and smaller grids, basis sets, and other details such as absorption were made at the start of this work. We estimate that the values finally chosen should lead to converged reaction probabilities to within 10%.

TABLE 1: Computational Details of the Reactive and Capture Wave Packet Calculations

parameters (au = atomic units)	reactive calculation	capture calculation
R_{min} (au), R_{max} (au), N_R	0.1, 13.0, 176	0.4, 14.0, 176
r_{HHmin} (au), r_{HHmax} (au), N_{HH}	0.5, 12.0, 76	1.0, 5.0, 48
number of r_{CH} PODVR points	2	1
largest value of j_{HH}	20[a]	16[a], 13[b]
largest value of j_{CH}	20	18
absorption parameters[c]: C_{abs} (au), R_{abs} (au) for *R*	10, 0.005	10.5, 0.005
absorption parameters: C_{abs} (au), R_{abs} (au) for *R*	9.0, 0.005	2.0, 0.005
absorption parameters: C_{abs} (au), r_{abs} (au) for r_{HH}	N/A	2.0, 0.1
absorption parameters: C_{abs} (au), R_{abs} (au) for *R* in the interaction region	0.35, 9.0, 0.3	0.3, 9.0, 0.3
incoming Gaussian function[d]: $\hbar^2k_o^2/(2\mu)$ (eV), R_0 (au), α (au)		

[a] The rotational basis for H_2 with initial $j_{CH} = j_{HH} = 0$. Note that only even values of j_{HH} are contained in the basis. [b] Used in the capture calculation with initial $j_{CH} = j_{HH} = 1$. Note that only odd values of j_{HH} are contained in the basis. [c] The absorption is given by $\exp[-C_{abs}(R - R_{abs})^2]$, $R \geq R_{abs}$, except in the interaction region where it is applied for $R \leq R_{abs}$. [d] Defined as in ref 13.

The capture probabilities are computed with wave packet methods by absorbing the wave packet as it enters into the interaction region, as described by Lin and Guo.[17,18] Because this calculation involves the entrance channel only, where coupling between various degrees of freedom is relatively weak, the basis sets required are somewhat more modest than for the full quantum calculation. Nevertheless, a rather large rotational basis is required for convergence. The capture probabilities are computed directly from a flux analysis. The flux is evaluated at a value of *R*, $R^\dagger$, that is, between the asymptotic region and the entrance channel. As long as $R^\dagger$ is not too close to the absorption region, the results are independent of its exact value. The results are also not very sensitive to the absorption parameters in the interaction region. Numerical parameters for the capture wave packet calculations are also given in Table 1.

2.3. Classical Trajectories. The VENUS96 trajectory program[19] was used to carry out our quasiclassical trajectory (QCT) work. The analogue of the $J = 0$ quantum calculations above is to run only collisions of CH and H_2 with zero impact parameter and ZPE in the respective diatomics. These calculations are carried out using a version of VENUS96 customized to incorporate the potential, with derivatives being calculated numerically. A time step of 0.05 fs is used, and initial and final separations of the collision fragments are taken to be 12 a_0. With initial energy $E_{ZPE} + E_{col} = 0.44$ eV + E_{col}, energy conservation to 4×10^{-5} eV is achieved. We study fixed collision energies E_{col} in the range 0.05 to 1 eV, integrating a sufficient number of trajectories for each E_{col} to yield reaction probabilities with statistical error ≤2%. This can require up to 12 000 trajectories at the lowest collision energies.

Of course in the case of QCT calculations, a variety of other calculations can be readily performed, and we have estimated the thermal rate constant at several temperatures in the range 300−1000 K using the Boltzmann distribution sampling methods within Venus. These methods sample the appropriate distributions of collision energies, impact parameters, and reactant rotational states. The reactants are kept in their vibrational ground states, which should be adequate for the temperatures studied. At each temperature, the number of trajectories is chosen so that the statistical error is less than 2%, which can involve between 31000 and 90 000 trajectories per

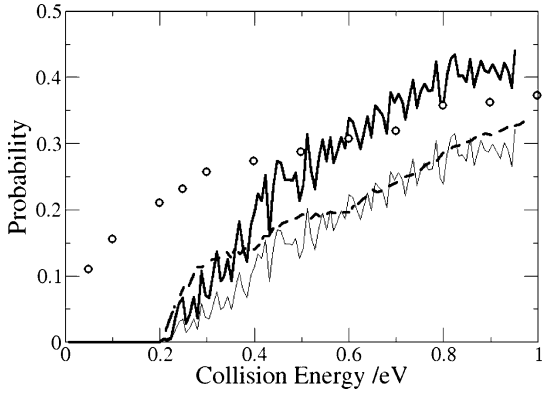

Figure 2. Total angular momentum $J = 0$ reaction probabilities for $CH + H_2 \rightarrow CH_2 + H$, with zero-point energy in the reactants: quantum dynamics model (heavy solid curve), quasiclassical trajectories (circles), capture/phase space theory model (dashed curve), and corrected quantum results (thin solid curve). Regarding fine structure in the quantum results, see the text for further discussion.

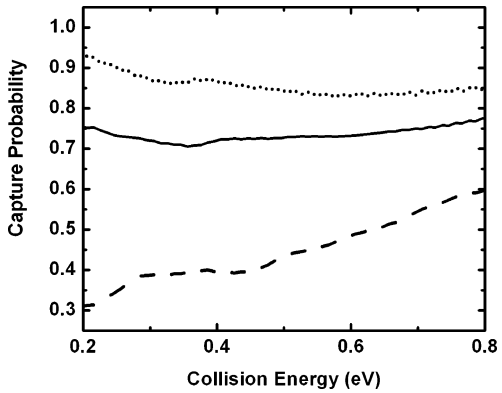

Figure 3. Capture probability as a function of initial translational energy for three different initial conditions: $j_{HH} = j_{CH} = 0$ (solid line); $j_{HH} = j_{CH} = 1$, $|k_{HH}| = |k_{CH}| = 0$ (dashed line); $j_{HH} = j_{CH} = 1$, $|k_{HH}| = |k_{CH}| = 1$ (dotted line).

temperature. The rate constant is computed from the total number of reactive trajectories based upon[20]

$$k(T) = g_{el}\sqrt{\frac{8k_BT}{\pi\mu}}\,\pi b_{max}^2\,\frac{N_r}{N} \qquad (1)$$

where N_r/N is the fraction of reactive trajectories, b_{max} is the maximum impact parameter, and μ is the reduced mass of H_2 and CH. We include an electronic degeneracy factor, $g_{el} = {}^1/_2$. This factor is needed because only one of the two spatial components of the Π state of CH in the reactants correlates with CH_3 and the $H + CH_2$ product channel. To converge the rate constant calculations, $b_{max} = 5.5$ Å and 15 000 trajectories were required at each temperature.

2.4. Capture/Phase Space Theory (C/PST) Statistical Model. In phase space theory (PST), as pioneered by Light and Pechukas,[21,22] a reaction probability is given by P_cP_s, where P_c is the probability of forming a complex and P_s is the probability for the complex to react weighting all available channels equally. (See ref 23 for a more recent discussion of PST.) Rather than estimate P_c in various approximate ways, we can use our wave packet-based capture probabilities (see section 2.2). Our procedure for evaluating the statistical probability P_s is detailed in the Appendix.

3. Results

3.1. Reaction Probabilities. The quantum mechanical (QM) reaction probability, P_r, for CH ($v_{CH} = j_{CH} = 0$) + H_2 ($v_{HH} = j_{HH} = 0$) $\rightarrow$ CH_2 + H, with total angular momentum $J = 0$, is shown in Figure 2 as the heavy solid curve. As discussed in section 2.2, our QM model results are likely overestimates of the true reaction probability, and the thin solid curve in Figure 2 is the corrected quantum probability, $\bar{P}_r$, result is given by applying eq A4 of the Appendix. The open circles with error bars are the corresponding quasiclassical trajectory (QCT) results. The dashed curve is the capture/phase space theory (C/PST) estimate of the reaction probability given by P_cP_s. We have taken $P_c = 0.74$, consistent with our capture wave packet calculations of section 3.2 below.

The C/PST and corrected QM results are in reasonable accord at moderate and high energies and show some larger discrepancies in the 0.2−0.4 eV range. Assuming the corrected QM results are a reasonable representation of the true situation, the results are consistent with statistical behavior of the CH_3 complexes, once they are formed. The zigzag features in the QM probabilities are due to the many overlapping resonances present, a feature common to the QM reaction probabilities of many complex-forming chemical reactions such as $H + O_2$.[24,25] The details of the zigzag patterns are sensitive to many parameters and are difficult to converge absolutely.[25] More fine structure will also result with use of a denser energy grid. We connected the QM points with lines in Figure 2 only for reasons of visual clarity.

The QCT results in Figure 2 are generally higher than the C/PST and QM results, with the largest discrepancies occurring for collision energies near and below the QM threshold for reaction, ≈0.2 eV. Note that the statistical errors (≤2%) in the QCT results are equal in size or smaller than the size of the symbols used and so are not shown. It turns out that there is no rigorous QCT threshold for reaction because the ZPE placed in the reactants, 0.44 eV, is greater than the minimum energy to form products classically. Because there is no barrier to reaction, this latter energy is just the classical endothermicity, 0.18 eV. Coupled with the presence of a deep well in the interaction region, and the fact that the ZPE of CH_2 (0.47 eV) is relatively large like the reactants, many trajectories with reactant ZPE and collision energy below 0.18 eV can react because they can form CH_2 with energy less than its ZPE. While ZPE violation is well-known, the energetic details just noted make the CH + H_2 reaction a particularly severe case. We will see in section 3.3 that the incorrect threshold behavior has severe consequences for the temperature dependence of the QCT rate constant.

3.2. Capture Probabilities. As shown in Figure 1, there are no barriers on the MEP. Thus, one might expect the capture probabilities (P_c) to be unity for all translational energies. At the energies relevant for the reaction, however, this turns out not to be the case. The solid line in Figure 3 gives the capture probabilities computed from the $J = 0$ calculation with initial $j_{HH} = j_{CH} = 0$. For translational energies in the range of 0.2−0.8 eV, the capture probability is in the 70−74% range. The reason that $P_c < 1$ is that the entrance channel is relatively narrow with respect to the orientations of the CH and the H_2. In Figure 4, we plot the potential energy as a function of θ_{HH} and θ_{CH} with $R = 4.8\ a_0$ ($R^\dagger$), and r_{CH}, r_{HH}, and φ at their equilibrium values. The diatomics are optimally oriented when they approach one another nearly parallel to each other and perpendicular to R. When both CH and H_2 are initially in the ground rotational state, there is a broad angular distribution in the entrance channel so that a significant portion of the wave packet is reflected back toward the reactants before it enters the complex region. Thus, one might expect P_c to be a function of the initial orientation of the diatomics. To test the effect of

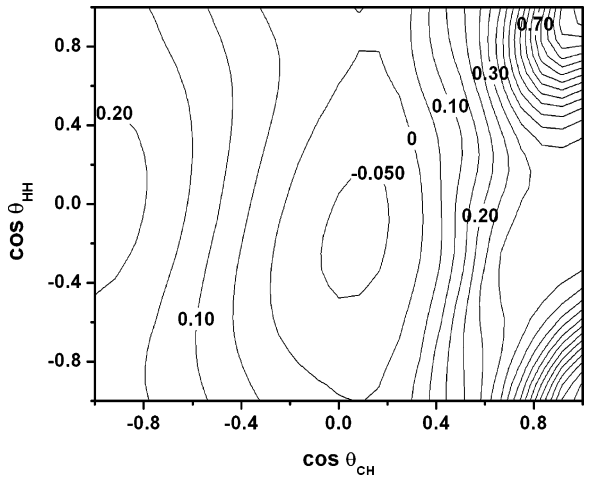

Figure 4. Contour plot of the potential energy surface as a function of θ_{HH} and θ_{CH}, with $R = 4.8\ a_0$, $\varphi = 0$, and the CH and H_2 bond lengths in their equilibrium positions. Contours range from −0.05 to 1 eV in increments of 0.05 eV.

this initial orientation, we computed the $J = 0$ capture probability with initial $j_{CH} = j_{HH} = 1$. When $J = 0$, the quantum numbers for projection of the angular momentum of the diatomics on the body fixed R axis, k_{CH} and $k_{HH,}$ are equal in magnitude and opposite in sign. For the initial condition, $j_{CH} = j_{HH} = 1$ the magnitude of k_{HH} can be either 0 or 1.[10] If $|k_{HH}| = |k_{CH}| = 0$, both diatomics will be aligned along the R axis so that CH and H_2 approach one another collinearly. If, however, $|k_{HH}| = |k_{CH}| = 1$, then, for both H_2 and CH, the initial rotational even-parity wave function is given by sin θ cos φ. Thus, the two diatomics face one another and are perpendicular to R, the most favorable orientation. We see from Figure 3 that this perpendicular orientation (dotted line) does indeed give rise to larger P_c and that the collinear orientation (dashed line) leads to much smaller values.

Thinking classically, we might suspect that there will be two basic types of trajectories in this reaction, those that enter the complex region and those that do not. The former trajectories form a highly excited CH_3 complex and may be expected to dissociate to one of the six product channels (three equivalent reactive channels and three equivalent nonreactive channels) in a statistical manner. We would expect that the distribution of trajectory lifetimes would be broad and that all three hydrogens would have an equal chance of ending up attached to the carbon atom. Those trajectories that do not enter the complex region however, would all be nonreactive, have short lifetimes, and there would be no exchange of H atoms. The distribution of trajectory lifetimes shown in Figure 5 illustrates this point. The lifetime distributions for the reactive trajectories, and for the nonreactive trajectories that exchange H atoms, are broad with very few with a lifetime of ≤0.2 ps. In contrast, 57% of the nonreactive trajectories that do not exchange H atoms are in the ≤0.2 ps range, representing 21% of the total number of trajectories. (If we assume that these trajectories are not "captured", then the quasiclassical capture probability is 0.79, somewhat higher than the quantum capture probability of 0.74.) We can further assess the statistical nature of the break up of the collision complex by comparing the number of reactive trajectories that exchange hydrogens and those that do not. (Note that the exchange channel is not included in our wave packet calculations.) If the breakup of the complex is statistical, then $^1/_3$ of all reactive trajectories should be in the exchange channel. For all of the energies considered here, this condition is satisfied within statistical error.

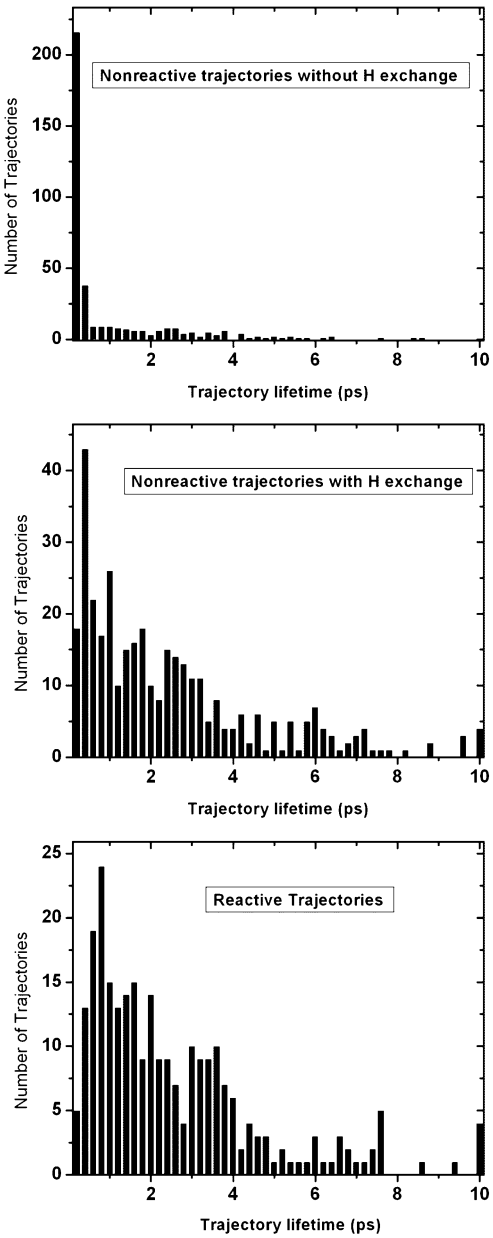

Figure 5. Lifetime distributions from the trajectory calculations.

We plan to make an extensive analysis of capture probabilities for total angular momentum states $J > 0$. To obtain a rough idea of the effect of J for the present paper, we performed some preliminary calculations for $J = 10$, 20, and 30, employing a smaller rotational basis, with 6 and 12 being the largest values of j_{HH} and j_{CH}, respectively. The reactants were kept in their ZPE states, and we used the helicity conserving approximation.[26] Since these results are not fully converged, we do not display them. However, we expect them to be accurate to within 10−15%. We find, in general, that centrifugal barrier effects tend to lower the capture probabilities, particularly at low collision energies. Nonetheless, the capture probabilities are still significant. For $J = 30$, for example, $P_c \approx 0.3$ at $E_{col} = 0.2$ eV, rising to $P_c \approx 0.7$ at $E_{col} = 0.5$ eV. This implies that $J = 30$ and higher values of J will make substantial contributions to the reactive cross sections at all relevant collision energies. We therefore anticipate that high values of J will contribute significantly to the thermal rate constants. This is also consistent with the large impact parameters ($b_{max} = 5.5$ Å, section 2.3) required to converge the QCT rate constants.

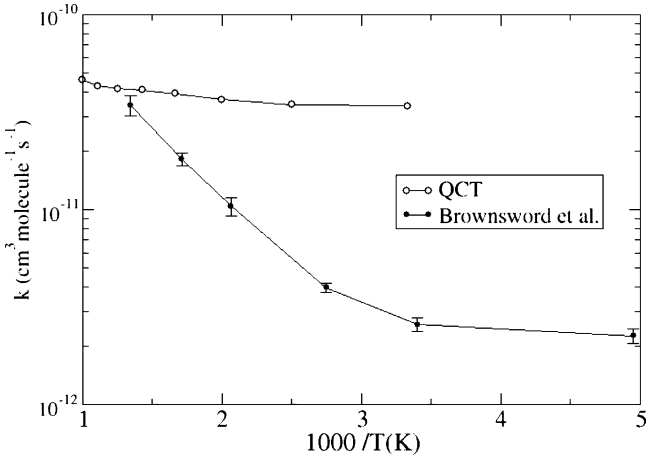

Figure 6. Arrhenius plot of the QCT rate constants, open symbols, and the experimental low-pressure rate constants of Brownsword et al., filled symbols.[3]

3.3. Rate Constants. It is possible to estimate a low-pressure rate constant using the quantum reaction probability of Figure 1. For example, one can determine, on the basis of the potential along the MEP and a $J(J+1)/(2\mu R^2)$ centrifugal term, various centrifugal barriers to complex formation from reactants. One can then proceed as in ref 27 by simply assuming the reaction probability for any total angular momentum, J, is of the same form as the $J = 0$ one but shifted in energy to account for the centrifugal barriers. These probabilities can then be used to compute cross sections and/or rate constants. However, this approach, even when corrected for the 0.055 eV error in the theoretical endothermicity, leads to an underestimation of the rate constants by 2 orders of magnitude at 300 K and 1 order of magnitude at 1000 K. The reason for this is that the reaction is sufficiently endothermic that relatively high E_{col} values, ≥ 0.2 eV, contribute to the rate constant. These energies are all above the low-J centrifugal barriers, making them irrelevant. Thus, the high-J centrifugal barriers, say for $J > 30$, are crucial in determining the magnitude of the rate constant. Owing to dynamical effects, these barriers are inadequately approximated with the simple procedure outlined here. The incorporation of more accurate J-dependent capture probabilities such as those discussed above may provide more reliable rate constants. It is also likely that the simple centrifugal-barrier capture model would be more quantitative when applied to reaction probabilities for the reverse reaction, $CH_2 + H \rightarrow CH + H_2$, which is exothermic.

For the present paper, we have, however, determined QCT-based rate constants. These rate constants were obtained as outlined in section 2.3, with statistical errors sufficiently small (2%) that the error bars lie with the size of the symbols used to present the results (open circles) in Figure 6. The figure also gives the experimental low-pressure rate constants of Brownsword et al. (filled circles).[3] The QCT rate constants do not follow the experimental trend at lower temperatures, that is, high 1000/T, and are essentially flat. As discussed in section 3.1 in relation to Figure 2, there can be unrealistically large QCT reactivity at collision energies near and especially below the correct quantum mechanical threshold due to a severe ZPE violation problem. This is responsible for the physically incorrect, flat QCT rate constant. However, it is encouraging that the higher temperature experimental and QCT results, or low 1000/T results, are in agreement. Of course, given the severe ZPE violation problems and the fact that 1000 K is not sufficiently high to ensure the classical limit has been achieved, this agreement may even be somewhat fortuitous and deserves further investigation (see Concluding Remarks).

4. Concluding Remarks

We carried out quantum and classical dynamics calculations on the $CH + H_2$ reaction with a recently developed global potential energy function.[9] Our results are consistent with a capture/phase space theory model with nonunit capture probabilities. The nonunit capture probabilities arise from angular constraints to complex formation, but collision complexes that do form behave statistically.

The limited nature of our quantum calculations did not permit a reliable quantum determination of the low-pressure rate constant. Future work will be to pursue a more complete quantum description of the problem to fully compare with statistical models. We will also apply more sophisticated capture-based approaches to estimating the rate constants in the spirit of the wave packet-based statistical methods of Lin and Guo.[17,18] This will be an extensive project that requires, for converged estimates, the determination of many capture probabilities in a suitable ensemble of total angular momentum states and initial diatomic rotational states.

Regarding the quasiclassical trajectory (QCT) results, we found that a severe ZPE violation problem led to significant error in the QCT-based rate constant. It would of interest to pursue approaches to incorporate ZPE effects by rejection of certain trajectories. Simply rejecting from consideration trajectories that have less than ZPE in the products is one very simple approach that guarantees the threshold energy will be correct and will lead to a more qualitatively correct temperature variation in the rate constant. Our preliminary calculations, however, indicate that the corresponding magnitudes of the rate constants are not satisfactory. More sophisticated approaches, as in the work of Varandas and co-workers on $H + O_2$,[28,29] and a much larger investigation beyond the scope of the present paper are required. Indeed, the severity of the problem in the present case may make it a very good test case for comparing and validating various ZPE correction approaches.

The exothermic reverse ($CH_2 + H \rightarrow CH + H_2$) reaction is somewhat easier to study theoretically and can lead to rate constants for the forward reaction as well via detailed balance. We therefore also plan to carry out quantum and classical calculations of this reaction. Finally, it will be interesting to apply variational transition state theory and related models[30] to the $CH + H_2$ system with the same potential surface as used here.

Acknowledgment. The work at Argonne National Laboratory was supported by the Office of Basic Energy Sciences, Division of Chemical Sciences, Geosciences, and Biosciences, U.S. Department of Energy, under Contract W-31-109-ENG-38. E.M.G. acknowledges support from the National Science Foundation. The work at Barcelona was supported by the Spanish MST (Project BQU2002-04269-C02-02) and Spanish MEC (Project CTQ2005-09334-C02-01), by the "Generalitat of Catalonia" (refs 2001SGR 00041 and 2005SGR 00175), and by C^4-CESCA/CEPBA. J.M. is also grateful to the Spanish Ministry of Education and Science for a predoctoral research grant. The work at Vitoria was supported by Spanish MCyT (Proyect BQU2002-04462-c02-02) and Spanish MEC (Proyect CTQ2005-09185-c02-01). We are grateful for many helpful discussions with Drs. L. B. Harding, S. J. Klippenstein, H. Guo, and D. M. Medvedev. We dedicate this work to John Light in appreciation of his many contributions to theoretical chemistry.

Appendix: Statistical Considerations

A capture/phase space theory estimate of the reaction probability is P_cP_s, where P_c is the probability to form complexes and P_s is a simple statistical reaction probability for the complex

$$P_s(E) = \frac{N_{CH_2}(E)}{N_{CH_2}(E) + N_{CH+H_2}(E)} \tag{A1}$$

with N_{CH_2} and N_{CH+H_2} being the total number of product and reactant internal states available at total energy E. It is possible to obtain these state numbers to be consistent with our $J = 0$, even-parity quantum calculations. In the case N_{CH+H_2}, one simply constructs it from only the primitive rotational quantum numbers used in the quantum calculation, that is, from all possible $J = 0$ even-parity rotational states superimposed on all possible reactant vibrational states. The number of available CH_2 states does not correspond to zero angular momentum for CH_2 since the orbital angular momentum associated with the outgoing H atom can add negatively to it from an overall zero total angular momentum. There are various ways to obtain N_{CH_2}, for example, the use of approximate rovibrational energy levels for CH_2 and careful consideration of angular momentum constraints. A simple numerical way, which we used, is to explicitly determine all the available CH_2 states consistent with a numerical representation of a triatom−atom Jacobi coordinates Hamiltonian with CH_2 and H infinitely separated and neglect radial kinetic energy terms associated with the CH_2−H distance. Essentially, the same Hamiltonian form and numerical implementation as in our diatom−diatom calculations is possible, and it is straightforward to apply the angular momentum constraints.[31] A Lanczos procedure similar to that of ref 32 was used.

The method of calculation of P_s outlined above involves enumerating all the possible reactants in one particular reactant channel, say $CH_a + H_bH_c$. Similarly, it involves enumerating all the possible products in one product channel, say, $H_aCH_b + H_c$. Considering hydrogen exchanges, there are actually three equivalent reactant channels and three equivalent product channels. Because of the equal number of reactant and product channels, however, eq A1 and its method of evaluation above are still valid for the general case that allows all possible hydrogen exchanges since all the absolute state numbers just triple and the ratios remain the same. In this paper, we also carried out some quantum reaction probability calculations starting from the $CH_a + H_bH_c$ channel and not permitting CH_a to dissociate, that is, not allowing completely free exchange of the hydrogen atoms. It is easy to see then that only one of the three reactant channels ($CH_a + H_bH_c$) and two of the three product channels ($H_aCH_b + H_c$ and $H_aCH_c + H_b$) are possible. Because of this imbalance, and assuming a strong statistical component to the reaction probability, one expects the corresponding quantum reaction probability to be an overestimate. For example, if the probability of forming complexes were unity and the complexes decayed completely statistically, then the correct reaction probability would be P_s from above. However, the restricted quantum problem has only $2N_{CH_2}/3$ of the possible product states and $N_{CH+H_2}/3$ of the possible reactant states. If the number of reactant channels greatly exceeds the number of product channels, then one would predict that the quantum probability is an overestimate by a factor of 2: $P_r \approx [2N_{CH_2}/3]/[N_{CH+H_2}/3] = 2\,P_s$.

For nonunit P_c, it is possible to obtain a better correction factor for the calculated quantum probabilities, as follows. First, we assume that a corrected quantum reaction probability is of the form

$$\bar{P}_r = P_c\,\bar{P}_s \tag{A2}$$

where P_c is computed via the wave packet method discussed in the text and $\bar{P}_s$ is to be found from

$$\bar{P}_s = \frac{(3/2)P_r}{(3/2)P_r + 3P_{nr}(\text{stat})} \tag{A3}$$

with P_r being the original quantum reaction probability based on the limited number of available channels and P_{nr}(stat) being the statistical part of the total nonreactive probability, P_{nr}. Since $P_{nr} = (1 - P_c) + P_{nr}(\text{stat}) = 1 - P_r$, we find $P_{nr}(\text{stat}) = P_c - P_r$. Equation A2 then becomes

$$\bar{P}_r = P_c \frac{P_r}{2P_c - P_r} \tag{A4}$$

With $P_c = 0.74$ and $P_r = 0.3$, for example, the corrected reaction probability given by eq A4 is 0.19, that is, 1.6 times smaller than the original value.

References and Notes

(1) Berman, M. R.; Lin, M. C. *J. Chem. Phys.* **1984**, *81*, 5743.

(2) McIlroy, A.; Tully, F. P. *J. Chem. Phys.* **1993**, *99*, 3597.

(3) Brownsford, R. A.; Canosa, A.; Rowe, B. R.; Sims, I. R.; Smith, I. W. M.; Steward, D. W. A.; Symonds, A. C.; Travers, D. *J. Chem. Phys.* **1997**, *106*, 7662.

(4) Liu, K.; Macdonald, R. G. *J. Chem. Phys.* **1988**, *89*, 4443.

(5) Eng, R. A.; Gebert, A.; Goos, E.; Hippler, H.; Kachiani, C. *Phys. Chem. Chem. Phys.* **2001**, *3*, 2258.

(6) Goos, E.; Hippler, H.; Kachiani, C.; Svedung, H. *Phys. Chem. Chem. Phys.* **2002**, *4*, 4372.

(7) Brooks, B. R.; Schaefer, H. F., III. *J. Chem. Phys.* **1977**, *67*, 5146.

(8) Dunning, T. H., Jr.; Harding, L. B.; Bair, R. A.; Eades, R. A.; Shepard, R. L. *J. Phys. Chem.* **1986**, *90*, 344.

(9) Medvedev, D. M.; Harding, L. B.; Gray, S. K. *Mol. Phys.* **2006**, *104*, 73.

(10) Goldfield, E. M.; Gray, S. K. *J. Chem. Phys.* **2002**, *117*, 1604.

(11) Ruscic, B. Private communication, 2005, obtained from Active Thermochemical Tables (ATcT), version 1.25, operating on the Core (Argonne) Thermochemical Network, version 1.047.

(12) Ruscic, B.; Pinzon, R. E.; Morton, M. L.; von Laszevski, G.; Bittner, S. J.; Nijsure, S. G.; Amin, K. A.; Minkoff, M.; Wagner, A. F. *J. Phys. Chem. A* **2004**, *45*, 9979.

(13) Gray, S. K.; Balint-Kurti, G. G. *J. Chem. Phys.* **1998**, *108*, 950.

(14) Echave, J.: Clary, D. C. *Chem. Phys. Lett.* **1994**, *100*, 402.

(15) Medvedev, D. M.; Goldfield, E. M.; Gray, S. K. *Comput. Phys. Commun.* **2005**, *166*, 94.

(16) Meijer, A. J. H. M.; Goldfield, E. M.; Gray, S. K.; Balint-Kurti, G. G. *Chem. Phys. Lett.* **1998**, *293*, 270.

(17) Lin, S. Y.; H. Guo, H. *J. Chem. Phys.* **2004**, *120*, 9907.

(18) Lin, S. Y.; H. Guo, H. *J. Phys. Chem A* **2004**, *108*, 10066.

(19) Hase, W. L.; Duchovic, R. J.; Hu, X.; Lim, K. F.; Lu, D. H.; Pelsherbe, G. H.; Swamy, K. N.; Van de Linde, S. R.; Wang, H.; Wolf, R. J. *Quantum Chem. Prog. Exch. Bull.* **1996**, *16*, 671.

(20) Truhlar, D. G.; Muckerman, J. T. *Atom-Molecule Collisition Theory: A Guide for the Experimentalist*; Bernstein, R. B., Ed., Plenum: New York, 1979; pp 595−646.

(21) Light, J. C. *J. Chem. Phys.* **1964**, *40*, 3221.

(22) Pechukas, P.; Light, J. C. *J. Chem. Phys.* **1965**, *42*, 3281.

(23) Larregaray, P.; Bonnet, L.; Rayez, J.-C. *J. Phys. Chem. A* **2006**, *110*, 1552−1560.

(24) Pack, R. T.; Butcher, E. A.; Parker, G. A. *J. Chem. Phys.* **1995**, *102*, 5998.

(25) Meijer, A. J. H. M.; Goldfield, E. M. *J. Chem. Phys*. **1998**, *108*, 5404.
(26) Pack, R. T. *J. Chem. Phys*. **1974**, *60*, 633.
(27) Gray, S. K.; Goldfield, E. M.; Schatz, G. C.; Balint-Kurti, G. G. *Phys. Chem. Chem. Phys*. **1999**, *1*, 1141.
(28) Varandas, A. J. C.; Brandao, J.; Pastrana, M. R. *J. Chem. Phys*. **1992**, *96*, 5137.
(29) Varandas, A. J. C. *J. Chem. Phys*. **1993**, *99*, 1076.
(30) Truhlar, D. G.; Garrett, B. C.; Klippenstein, S. J. *J. Phys. Chem*. **1996**, *100*, 12771.
(31) Gatti, F.; Iung, C.; Menou, M.; Chapuisat, X. *J. Chem. Phys*. **1998**, *108*, 8821.
(32) Gray, S. K.; Goldfield, E. M. *J. Phys. Chem. A* **2001**, *105*, 2634.